Proceedings of the ASME 2021
Fluids Engineering Division Summer Meeting
FEDSM2021
August 10-12, 2021, Virtual, Online

FEDSM2021- 65771

COMPUTAIONAL FLUID DYNAMIC ANALYSIS OF THE FLOW AROUND A PROPELLER BLADE OF MULTIROTOR UNMANNED AERODYNAMIC VEHICLE

Victor H. Martinez
Graduate Student, Mechanical Engineering
University of Texas, San Antonio, USA

Kiran Bhaganagar
Professor, Mechanical Engineering
University of Texas, San Antonio, USA

ABSTRACT

Multirotor Unmanned Aerodynamic Vehicles (MUAV) have been a high interest topic in the aerodynamic community for its many applications, such as, logistics, emergency rescue, agriculture data collection, and environmental sensing to name a few. MUAV propeller blades create a highly complex turbulent fluid flow around the body and the environment around it. The flow physics generated from the rotation of the propeller blades were studied in this paper along with the analysis of aerodynamic characteristics. A Reynolds Average Navier-Stokes (RANS) Computational Fluid Dynamics (CFD) analysis of a propellor blade from a MUAV has been performed to quantify the aerodynamic effects. For this purpose, the verification and validation of the commercially available CFD solver COMSOL Multiphysics v5.5 was performed using the NACA 0012 airfoil which is one of the most highly studied of the NACA family. With this validation it created confidence on the results for simulating a MUAV propeller and evaluate the aerodynamic characteristics of thrust coefficient (K_T), power coefficient (K_P), and Efficiency (η). These characteristics were compared against experimental data and results showed to have a similar trend. This showed that the CFD solver is capable of solving the aerodynamic characteristics of any propeller blade geometry.

NOMENCLATURE

C_P	Pressure Coefficient
C_L	Lift Coefficient
C_D	Drag Coefficient
D	Characteristic Length Propeller Diameter
K_T	Thrust Coefficient
K_Q	Torque Coefficient
K_P	Power Coefficient
J	Advance Ratio
η	Propeller Efficiency
MUAV	Multirotor Unmanned Aerial Vehicle
Pa	Pascal (N/m^2)
Re	Reynold's Number
k	Turbulent Kinetic Energy
ε	Turbulent Dissipation Rate
U	Free Stream Velocity (m/s)
α	Angle of Attack (deg)
Ω	Rotational Speed (RPM)
ρ	Fluid Density (kg/m^3)
μ	Fluid Dynamic Viscosity (Pa·s)

1. INTRODUCTION

In the past few decades Multirotor Unmanned Aerial Vehicles (MUAV) have been used for many applications, such as, emergency rescue, agriculture data collection of meteorological variables, and logistics to name a few [1]. Although the recent high interest of use of MUAV, they can be very complex in many aspects. In particular, MUAV rely on the power and thrust generated by the rotating propeller blades in order to navigate. The propeller blades on a MUAV are composed of different camber and chord size airfoils along the spanwise direction of the blade. The combination of airfoils make up a single propeller and thus determine how effective the propeller will be under certain conditions. Based on Bernoulli's principle, due to the rotation of the propeller, an acceleration of airflow over the surface is generated, which causes a reduction of static pressure in the front of the propeller. Meanwhile, lower speed at the back of the propeller causes to experience higher static pressure. This pressure difference creates the thrust force allowing the propeller to overcome drag resistance [2]. Most basic propellers include at least two blades connected by a hub at the center, which can allow the propeller to either rotate clockwise or counter-clockwise [3]. By looking further, the propeller blades create highly complex fluid flow characteristics in which are yet to be fully understood. The fluid flows generated by the rotating propeller create areas of high turbulence around

© 2019 by ASME

the propellers and body of the MUAV. These high turbulence areas generated can cause unpredictable behavior for the MUAV and result in control loss, which may result in negative consequences around its surroundings. Therefore, it is a significant interest in the fluid dynamics field of study to research the fluid flow characteristics generated by the rotating propellers. The best known methods used to study fluid flow problems are theoretically, experimentally, and numerically. In this study, the numerical approach of computational fluid dynamics (CFD) has been used to study the fluid flow of a single blade propeller to evaluate the aerodynamic characteristics such as, velocity, pressure distribution, coefficients of thrust, power, lift, and drag. A lot of research has been done for these parameters for aerodynamic purposes on the NACA airfoils and helicopter rotating blades, but not a lot has been done on MUAV propeller blades. Patel et al. [4] have performed CFD analysis to calculate the lift and drag forces on the NACA 0012 airfoil at various angles of attack (AOA), which were compared against other experimental data and showed close agreement. Thus suggesting a reliable alternative to performing experiments to calculate lift and drag forces. Rahman et al. [5] studied fluid flow characteristics for a flow over a propeller used in vertical takeoff and landing (VTOL) aircrafts using CFD in order to calculate thrust generated by the various rotation speed. Schenk [6] uses CFD to validate and verify the CFD solver chosen for that study on a single propeller blade and compare to experimental data [7]. Once the solver was validated, a rotor-on-rotor interaction study was performed to evaluate the effect of rotor separation and noise of propeller blades. Brandt et al. [7] conducted a full scale experimental research study on various propeller blades for MUAV and were performed at low Reynolds number (Re) ranging from 5,000 to 100,000 based on the propeller chord at 75% propeller blade diameter. The propeller diameters ranged from 9 to 11 inches. The different Re number was varied by altering the rotation speed of the propeller inside the wind tunnel apparatus ranging from 1500 to 7500 rpm. It was found that the design of the propeller plays a huge factor when considering the efficiency of the propeller for a MAUV. This proves that using CFD can be used to further explore various propeller shapes and find a more efficient design for a MUAV operating under certain conditions. With a higher availability of computational resources than in the past, CFD has become a far more cheaper, faster, and accurate method of choice in solving fluid flow problems. Therefore, it is a crucial tool in solving fluid flows for product design and optimization. A similar approach in this study was used from both of these studies [5][6] using the Moving Reference Frame (MRF) method to create the effect of a rotating geometry within the CFD simulations and evaluate the aerodynamic characteristics of a single propeller blade using the commercially available COMSOL Multiphysics v5.5 solver. COMSOL is a reliable Multiphysics solver used in industry and academia to solve various physic problems. For this study only the CFD module was used to study the fluid flow over the single propeller blade. COMSOL CFD module resolves the Reynolds-Averaged Navier-Stokes (RANS) partial differential equations using the finite volume method (FVM). Before any CFD results can be used for any application, the solver must be verified and validated against experimental data or previous numerical simulations who have also been validated. In this study the COMSOL CFD solver was validated by simulating the NACA 0012 airfoil and compared against experimental data [8]. Once the solver was validated the aerodynamic characteristics of thrust coefficient (K_T), power coefficient (K_P), torque coefficient (K_Q), lift coefficient (C_L), and efficiency coefficient (K_η) at various advance ratios (J) were evaluated.

2. OBJECTIVES

The objectives of this study are as follows: (1) Perform a validation and verification of the COMSOL Multiphysics CFD solver against experimental data for the NACA 0012 airfoil and its aerodynamic characteristics of coefficients of pressure, C_P, lift, C_L, and drag, C_D. This validation would then allow us to perform the next objective. (2) Perform an aerodynamic study of a single propeller blade and evaluate the performance against experimental data of another propeller blade. This will give confidence in the CFD solver on its capabilities of performing numerically simulations on rotating propeller blades for aerodynamic studies, which have little known literature available, and this study can expand on the research of numerical solutions of a MUAV.

3. METHODOLOGY

In this section we will discuss the methods used to numerically simulate the single blade propeller of a MUAV using CFD. For this study, the commercially available COMSOL Multiphysics v5.5 CFD module was used for its capabilities of solving rotating single phase fluid flow problems. Since the rotation of the single propeller blade had a low Reynold's number (Re), it was assumed that the operating conditions were well under Ma < 0.3. Therefore, the RANS incompressible equations were used to resolve the fluid flow around the propeller and evaluate the single blade propeller aerodynamic characteristics.

3.1. Propeller Blade Model

In this section we explain the geometric details of the propeller that was used in this CFD study. The propeller model used for this study was created using the 3D CAD modeling software, SolidWorks, and can be seen in Figure 1 below. The propeller diameter, D, was set to 50mm which was also chosen as the characteristic length. Propeller blade geometries are composed of a series of airfoils which are chosen based on the desired aerodynamic characteristics for the given application. For the propeller of choice, a series of airfoils along the spanwise direction were used to create this propeller and connected using the loft feature in the CAD software. The details of the airfoil chord lengths and pitch angles along the spanwise direction of the single blade propeller are summarized in Table 1.

© 2019 by ASME

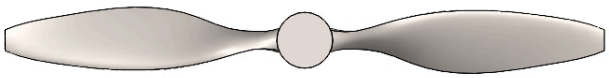

FIGURE 1: SINGLE BLADE PROPELLER MODEL

TABLE 1: AIRFOIL CHORD LENGTHS AND PITCH ANGLES

Radii (r/R)	Chord (c/R)	Pitch (deg)
0.15	0.139	65
0.25	0.186	60
0.35	0.233	45
0.85	0.163	20
1.0	0.070	5

3.2 Computational Domain

In order to successfully simulate the fluid flow around the propeller a computational fluid domain was created using a similar method described from these studies [5][6][9]. The entire fluid domain can be seen in Figure 2. The outer domain, that will act as a static body, has a diameter of 10D. With the upstream distance being 10D from the center of the propeller and an additional 20D downstream from the center of the propeller. The upstream and downstream distance selection is important to prevent any recirculation of the flow which can cause errors or convergence issues. In addition, the propeller blade is enclosed in a "puck" with a diameter of 1.1D and a thickness of 0.3D which is set as the rotating domain and can be set to rotate at any desired rotation speed. Furthermore, in order to improve solution convergence and capture the fluid flow physics that are being generated by the rotating propeller blade, a refinement region was added around the rotating domain. This refinement region creates a smoother mesh size transition from the rotating domain, which has finer mesh elements nears propeller wall, to the static domain, where mesh elements are much coarser towards the wall of the static domain. The domain details created for this study are summarized in Table 2.

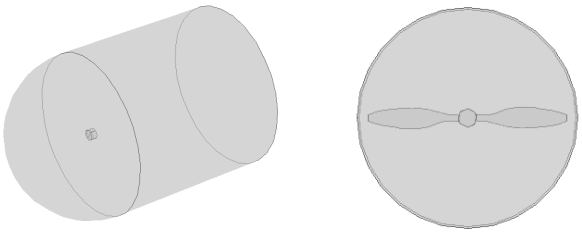

FIGURE 2: LEFT: COMPUTATIONAL DOMAIN. RIGHT: ROTATING DOMAIN ENCLOSING PROPELLER BLADE.

TABLE 2: SIMULATION DOMAIN DETAILS

Region	Dimension	Value
Propeller Diameter	D	50mm
Static Domain Diameter	10D	500mm
Static Domain Upstream	10D	500mm
Static Domain Downstream	20D	1000mm
Rotating Domain Diameter	1.1D	55mm
Rotating Domain Thickness	0.3D	15mm
Refinement Region Diameter	1.25D	62.5mm
Refinement Region Thickness	1.5D	75mm

3.3 Governing Equations

The governing equations used to simulate the single blade propeller are described by the incompressible RANS equations as described below. It is assume that the operating conditions for the rotating propeller are well under Ma < 0.3, allowing for an incompressible flow assumption. For incompressible flows the fluid density has a known constant therefore the continuity equation can be described using Equation 1.

$$\rho\nabla \cdot \mathrm{u} = 0 \tag{1}$$

For incompressible flows the conservation of momentum or Navier-Stokes equations can be written as seen in Equation 2.

$$\frac{\partial \mathrm{u}}{\partial t} + (\mathrm{u} \cdot \nabla)\mathrm{u} = -\frac{1}{\rho}\nabla pI + \nu\nabla^2\mathrm{u} + \mathrm{F} \tag{2}$$

In addition to the conservation of mass and momentum equations, there is also the turbulence equations to consider when solving for a turbulent fluid flow problem. In this study, the standard two equation *k-ε* turbulence model was chosen for its high use in fluid flow problems and least computationally demanding. The equations solved by the turbulent flow, *k-ε* interface are the continuity equation for conservation of mass and the RANS equations for conservation of momentum. The *k-ε* model introduces two additional transport equations and two dependent variables. The two new dependent variables are the turbulent kinetic energy, *k,* and the turbulent dissipation rate, *ε.* The standard *k-ε* turbulence model in the COMSOL CFD module is further described below.

The transport equations for the turbulent kinetic energy, *k,* and the turbulent dissipation rate, *ε*, are shown in Equations 3 and 4.

$$\rho\frac{\partial k}{\partial t} + \rho u \cdot \nabla k = \nabla \cdot \left(\left(\mu + \frac{\mu_T}{\sigma_k}\right)\nabla k\right) + P_k - \rho\varepsilon \tag{3}$$

$$\rho\frac{\partial \varepsilon}{\partial t} + \rho u \cdot \nabla \varepsilon = \nabla \cdot \left(\left(\mu + \frac{\mu_T}{\sigma_\varepsilon}\right)\nabla \varepsilon\right) + C_{\varepsilon 1}\frac{\varepsilon}{k}P_k - C_{\varepsilon 2}\rho\frac{\varepsilon^2}{k} \tag{4}$$

Additionally the turbulent viscosity, μ_T, and production term, P_k, in the above equations are modeled as seen in Equations 5 and 6.

$$\mu_T = \rho C_\mu \frac{k^2}{\varepsilon} \tag{5}$$

$$P_k = \mu_T\left(\nabla u: (\nabla u + (\nabla u)^T) - \frac{2}{3}(\nabla \cdot u)^2\right) - \frac{2}{3}\rho k\nabla \cdot u \tag{6}$$

The turbulence model constants for Equations 3-6 were kept at the default settings and are listed in Table 3 below. The constants

© 2019 by ASME

for the k-ε turbulence model were determined from experimental data [12].

TABLE 3: TURBULENCE MODEL CONSTANTS

Constant	Value
C_μ	0.09
$C_{\varepsilon 1}$	1.44
$C_{\varepsilon 2}$	1.92
σ_k	1.0
σ_ε	1.3

3.4 Meshing

The meshing grid was generated using the COMSOL v5.5 mesh tool that is built into the software. Creating a mesh is the next important step when setting up a CFD simulation as it determines how accurate the solution will be. Also, a solution may converge faster than a poorly created mesh. The quality of the meshing grid directly influences the rate of convergence, accuracy of solution, and computational time to obtain a solution. In this study, it was ensured that a finer mesh was created along the surface of the propeller, while the mesh towards the outer static domain had a coarser mesh. This would allow for a more accurate solution near the propeller while reducing computational time with fewer meshing elements. To further decrease the number of elements and reduce computational time, while keeping a relatively finer mesh, the domains described in Section 3.2 was split into sections along the rotating axis as shown in Figure 3. It was assumed that the effects of the rotating propeller will be symmetric along the axis of rotation. The forces that were calculated from the simulation will be multiplied by 2 to obtain the results of an entire propeller since we are simulating half of the propeller.

Both rotating domain and static domain consisted of unstructured tetrahedrons. The use of unstructured tetrahedron elements are best for complex geometry with high curvatures such as a propeller blade in this case. The mesh created around the propeller and rotating domain can be seen in Figure 3.

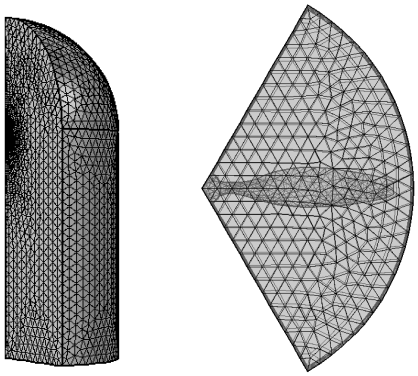

FIGURE 3: LEFT: TETHAHEDRAL MESH ON SPLIT DOMAIN. RIGHT: TETHAHEDRAL MESH ON PROPELLER AND ROTATING DOMAIN

In addition, a boundary layer (BL) mesh was created around the propeller blade. This would allow for the CFD simulation to resolve the physics as close to the propeller wall as possible. In order to ensure that the mesh created was of good quality, a feature within COMSOL allowing for mesh quality check was utilized. This is done by evaluating the skewness of each individual cell and gives it a rating between 0 and 1, where 0 is for bad quality cells and 1 is for good quality cells. Due to the high curvature of the propeller blade, it is more difficult to obtain perfect mesh elements around the surface, but nonetheless it is important to obtain the best mesh quality possible. Figure 4 shows the mesh quality along with the mesh quality rating scale. The mesh can be further improved, but in this case the quality was good enough for the solution to converge and arrive to an accurate result. The meshing statistics for this simulation are summarized in Table 4.

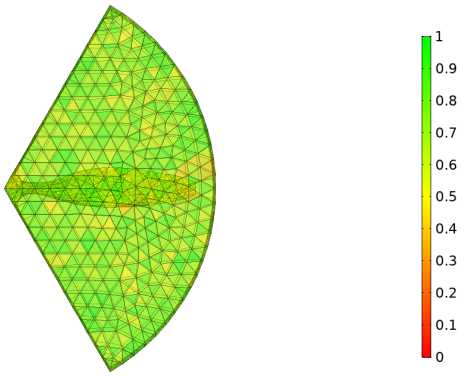

FIGURE 4: MESH ELEMENT QUALITY

TABLE 4: MESH GRID DETAILS AND STATISTICS

Mesh Element Type	Tetrahedra
No. of Elements	2,174,629
Max. Cell Size	0.0151 m
Min. Cell Size	1.32×10^{-4} m
Growth Rate	1.08
No. of BL Elements	50
BL Stretch Factor	1.2
Min. Element Quality	0.16
Ave. Element Quality	0.66

3.5 Boundary Conditions

The boundary conditions for this study consisted of a free-stream inlet at the spherical top end, a pressure outlet at the bottom end, a no slip wall condition on the propeller blade, and a symmetry condition on the walls of the outer domain. An internal domain enclosing the propeller blade was created in order to simulate the rotating region. The moving reference frame (MRF) approach was used in this study along with a frozen rotor study, which simulates as if the propeller is rotating but remains still. This interface connects the static and rotating domain together where a flow continuity condition was defined. Finally, since the domain was split a periodic flow condition was applied. A constant angular velocity of 3008 RPM was specified for the rotating domain in order to reach a steady state solution. With the specified angular velocity, flow conditions operated at

© 2019 by ASME

a Re of about 26,100. The simulation flow conditions for this study were taken from the UIUC data base [7] to compare against the experimental data for the advanced precision composite (APC) slow flyer propellers. The advance ratio coefficient, J, was used to determine the free-stream inlet velocity and evaluate the propeller aerodynamic characteristics and performance for different cases. The specified inlet velocities flow conditions are shown in Table 5.

TABLE 5: SIMLUATION INLET FLOW CONDITIONS

Advance Ratio, J	Inlet Free-Stream Velocity (m/s)
0.192	0.481
0.236	0.592
0.282	0.707
0.334	0.837
0.383	0.960
0.432	1.083
0.486	1.218
0.527	1.321
0.573	1.436
0.628	1.574
0.659	1.652
0.717	1.797
0.773	1.938
0.799	2.003
0.862	2.161
0.911	2.284

4. VALIDATION AND VERIFICATION

In order to be confident on the results obtained in a CFD solver a validation and verification study must be performed. Validation and verification for the NACA 0012 airfoil was conducted by evaluating the aerodynamic characteristics of the pressure coefficient, C_P, lift coefficient, C_L, and drag coefficient, C_D. In this section of the study, the validation of results are compared to experimental data obtained from Ladson [8]. The key in obtaining a well-defined solution in CFD is to be able to validate the solution is accurate and verify the solution with other experimental data or numerical solutions. Ideally, this should be compared against analytical solutions, but in many cases only experimental data is available. In this case, the NACA 0012 is a well-studied airfoil and has many experimental data and numerical solutions available for comparison. The steps taken to set up the validations and verification case for the NACA 0012 airfoil can be found here [10]. As it can be seen there is great agreement between Ladson's airfoil experimental data against the COMSOL CFD results. With the validation of the CFD code verified it can give confidence that it is a sound method in obtaining similar results on a single blade propeller.

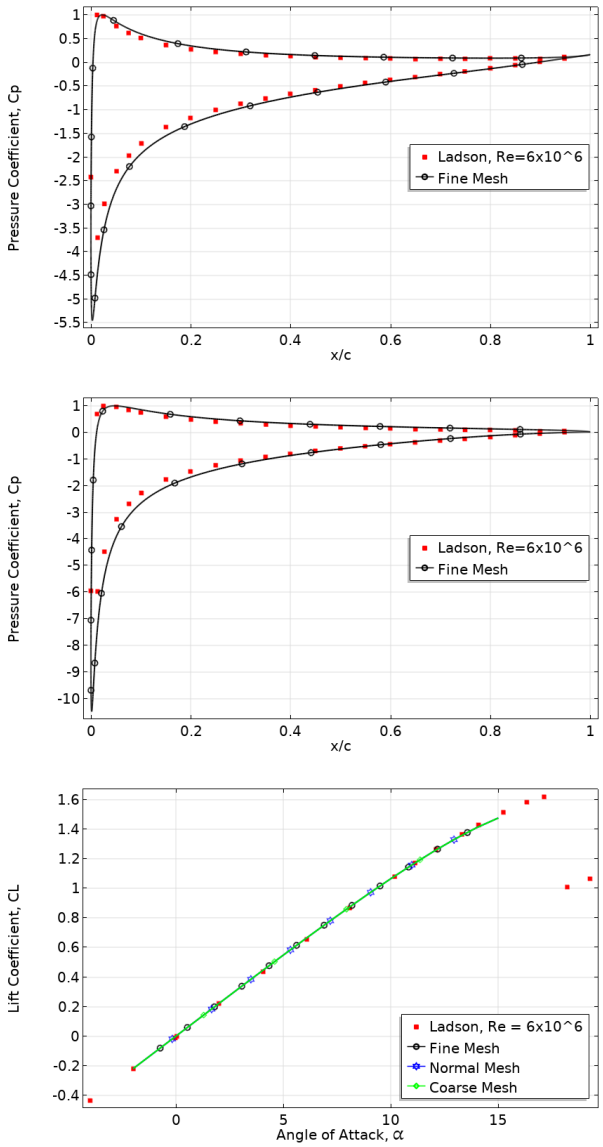

FIGURE 5: TOP: PRESSURE COEFFICIENT VS X/C FOR AOA=10. MIDDLE: PRESSURE COEFFICIENT VS X/C FOR AOA=15. BOTTOM: LIFT COEFFICIENT VS AOA.

5. RESULTS AND DISCUSSION

Numerical analysis results were compared to available experimental data in order to determine the quality and accuracy of the solutions. In order to quantify the numerical results we can calculate the axial force and momentum generated around the propeller, which are the thrust and torque, respectively. Equations 7-11 were used to calculate the aerodynamic performance of the single blade propeller. Where K_T is the thrust coefficient, K_Q is the torque coefficient, K_P is the power coefficient, J is the advance ratio, and η is the propeller efficiency.

$$K_T = \frac{T}{\rho \Omega^2 D^4} \tag{7}$$

© 2019 by ASME

$$K_Q = \frac{Q}{\rho \Omega^2 D^5} \quad (8)$$

$$K_P = 2\pi K_Q \quad (9)$$

$$J = \frac{U}{\Omega D} \quad (10)$$

$$\eta = \frac{K_T J}{K_P} \quad (11)$$

After performing the simulations under the fluid flow conditions described in Section 3.5 Table 5, we were able to obtain the results and compare against available experimental data [7]. The aerodynamic characteristic values calculated using Equations 7-11 were compared against various advance ratios and plotted against experimental data. Figure 6 shows the results of the single blade propeller. By further analyzing, the thrust coefficient, K_T, of the single blade propeller shows to under predict up to an advance ratio of 0.659, thereafter it shows to overpredict. The power coefficient, K_P, was overpredicted for all advance ratios in this case. Finally, the propeller efficiency, η, was underpredicted as well. There is room for improvement in this simulation study, but this also shows that the methodology used in this study can solve the aerodynamic performance for any propeller. In this case, the propeller of choice had different results to that of the APC slow flyer propeller. It can be further seen that the propeller created is much less efficient than the propeller it was compared against. Alternatively, it did produce more power, but did not efficiently use it to generate enough thrust. This can be due to the design of the propeller.

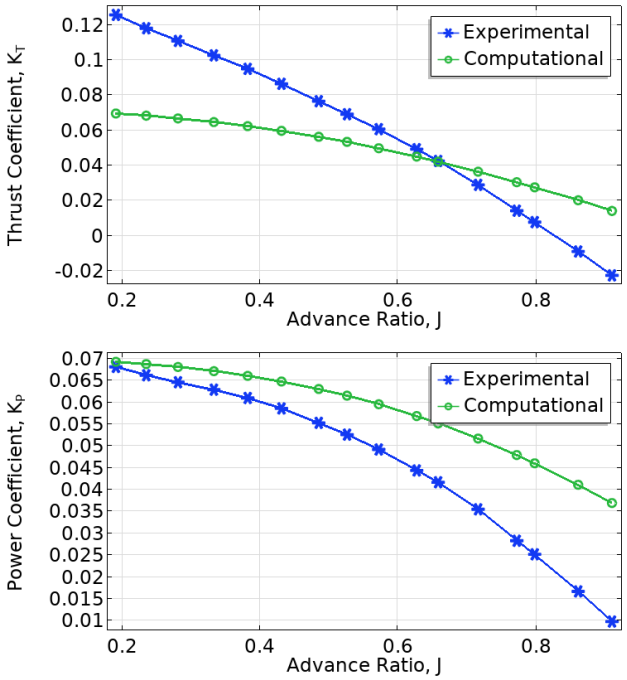

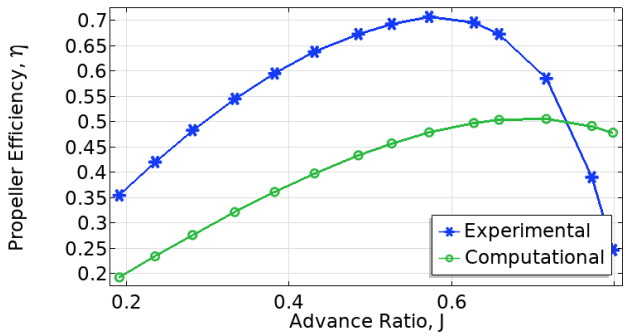

FIGURE 6: TOP: THRUST COEFFICIENT VS. ADVANCE RATIO. MIDDLE: POWER COEFFICIENT VS ADVANCE RATIO. BOTTOM: PROPELLER EFFICIENCY VS. ADVANCE RATIO.

From the simulation results, we were able to obtain the pressure distribution on the surface of the propeller. Figure 7 shows the pressure difference experienced by the rotation of the propeller at 3008 RPM along with the flow conditions of J=0.383. By further examining, from Bernoulli's principle, due to the rotation of the propeller an acceleration of airflow over the surface is generated, which causes a reduction of static pressure in the front of the propeller. Meanwhile, lower speed at the back of the propeller causes to experience higher static pressure. This pressure difference creates the thrust force allowing the propeller to overcome drag resistance. The max pressure experienced by the propeller under these flow conditions was 13.5 Pa at the bottom, while a minimum of -20.9 Pa was experienced at the top.

Additionally, from the same flow conditions of J = 0.383, we are able to see the velocity contours generated by the rotating propeller. Figure 8 shows how the thrust generated from the propeller creates a high stream velocity directly underneath it. With a max velocity of around 4 m/s created close to the propeller blades. We can also see a velocity of 0 m/s due to the no slip condition on the wall of the propeller at the hub.

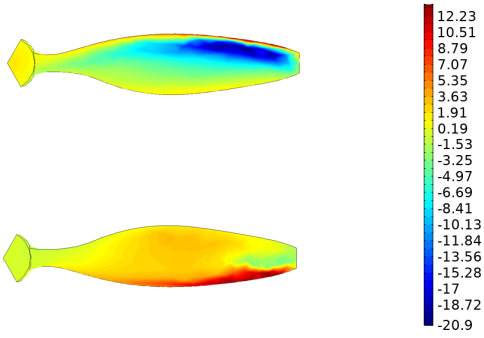

FIGURE 7: PRESSURE CONTOUR ON PROPELLER BLADE FOR J = 0.383. TOP: PRESSURE ON TOP OF PROPELLER. BOTTOM: PRESSURE ON BOTTOM OF PROPELLER.

© 2019 by ASME

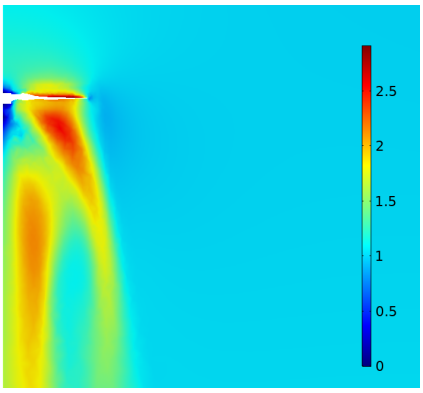

FIGURE 8: VELOCITY CONTOUR GENERATED FROM ROTATING PROPELLER FOR J = 0.383.

6. CONCLUSION

We discussed the background of the propeller blades for a MUAV and gave a brief literature review on previous studies done on MUAV propellers. In this study, the commercially available CFD solver COMSOL v5.5 was used and validated using the NACA 0012 airfoil in order to be certain this would be a sound method to use in simulating the propeller blade. A CFD analysis on a single blade propeller was performed and characterized its aerodynamic performance against experimental data of a APC slow flyer propeller. The methodology used in this study proved to show that the CFD solver is capable of solving external flow on rotating geometries. The outcome in this study, for the propeller model created, showed overpredicted and underpredicted results to that of the APC propeller experimental data. Nonetheless, It can be certain that any propeller geometry can be simulated and obtain good approximate results. Note, the propeller used in this study was created in a CAD modeling software, which has no experimental data available to compare directly. In future work, the APC propeller that was compared against will be created in the CAD modeling software and replace the propeller in this study, to compare to its experimental data. Also, different turbulence models available can be utilized and compared to determine which is more suitable for these applications. Finally, a mesh convergence study can be performed in order to determine the optimum mesh selection for these types of simulations. Furthermore, a variety of different propeller models operating at different RPM speeds can also be studied using the methodologies presented here. The possibilities are endless with the potential in furthering the research of MUAV using numerical simulations.

REFERENCES

[1] Christodouloi, K., et al. “Aerodynamic Analysis of a Quadcopter Drone Propeller with the Use of Computational Fluid Dynamics,” Chemical Engineering Transactions, 76, 181-186, 2019.

[2] Patel, Y., M.T. “CFD Analysis of Propeller Blade Design for Quadrotor,” Delhi Technological University, 2016.

[3] Delp, F. “Aircraft Propellers and Controls,” 1st ed., Jeppesen: Frankfurt, Germany, 1979.

[4] Patel, Karna S., et al., “CFD Analysis of an Aerofoil,” International Journal of Engineering Research, Vol. No. 3, Issue No. 3, pp 154-158, 2014.

[5] S. M. Mahbodur Rahman, et al. “Simulation Investigation on Flow Characteristics for the Flow Over a Propeller Used in VTOL RC Aircrafts,” International Conference on Mechanical, Industrial and Energy Engineering, 2014.

[6] Schenk, A. R., Theses and Dissertations, “Computational Investigation of the Effects of Rotor-on-Rotor Interactions on Thrust and Noise,” Brigham Young University, 2020.

[7] Brandt, J. B., “Small-Scale Propeller Performance at Low Speeds,” M.S. Thesis, University of Illinois at Urbana-Champaign, Urbana, IL, 2005.

[8] Ladson, C. L., “Effects of Independent Variation of Mach and Reynolds Numbers on the Low-Speed Aerodynamic Characteristics of the NACA 0012 Airfoil Section,” NASA TM 4074, 1988.

[9] Kutty, H. A., “3D CFD Simulation and Experimental Validation of Small APC Slow Flyer Propeller Blade,” Aerospace, 4(1), 10, 2017.

[10] COMSOL Multiphysics v5.5 “Flow Around an Inclined NACA 0012 Airfoil”

[11] COMSOL Multiphysics v5.5 CFD Module User Guide Chap. 3 pg. 186-190.

[12] D.C. Wilcox, “Turbulence Modeling for CFD,” 2nd ed., DCW Industries, 1998.

© 2019 by ASME